Kim *et al. Robomech J (2017) 4:5*
DOI 10.1186/s40648-017-0074-6

ROBOMECH Journal

RESEARCH ARTICLE

Open Access

Analysis of rotational flow generated by circular motion of an end effector for 3D micromanipulation

Eunhye Kim[1*†], Masaru Kojima[1‡], Liu Xiaoming[2], Takayuki Hattori[1], Kazuto Kamiyama[1], Yasushi Mae[1] and Tatsuo Arai[1]

Abstract

This paper presents a non-contact manipulation method using rotational flow generated by high speed motion of a glass needle. In order to generate an applicable motion that can precisely control the speed and position of a target object around an end effector, a manipulator actuated by three piezoelectric actuators is proposed. A compact parallel link produces precise three-dimensional motions. To reach the required end-effector frequency and amplitude, which is necessary for generating the rotational flow that can make rotational movement of microbeads having patterned data, the end effector motion is generated by controlling the three piezoelectric actuators at high speed. In this paper, we focus on rotational flow created by two-dimensional circular motion of the end effector mounted on the parallel link. By changing the amplitude and frequency of the circular motion, the generated swirl flow is analyzed in 3D space using 9.6-μm microbeads. We analyzed the velocity toward to the root of the end effector and angular velocity around the end effector by formulating models. From the analyzed data, we verified that the rotational flow has potential to manipulate micro-objects precisely in 3D space.

Keywords: Micromanipulation, High speed end effector motion, Piezo-actuator, Rotational flow

Background

In recent years, micromanipulation systems have become widely used in various applications such as manipulating biological cells or microorganisms, assisting micro-surgical operations, and assembling micro devices. To deal with different types of microobjects including biological cells and microparts, many manipulation methods have been proposed. The manipulation techniques can be classified in two ways: contact manipulation and non-contact manipulation [1].

Contact manipulation is mechanical manipulation by direct contact with target objects. Avci et al. and Zhang et al. presented high-speed autonomous manipulation of microshperes utilizing a two-fingered microhand [2] and a MEMS microgripper [3, 4], respectively. The main advantage of contact manipulation techniques is that physical approaches such as cutting, injecting, and stimulating can be achieved precisely. For example, Yamanishi et al. [5] succeeded in enucleation of oocyte by cutting the surface of the oocyte. Huang et al. [6] applied an automated micro-robotic system for cell injection. Motoyoshi et al. [7] proposed a local environmental stimulation system using two pipettes controlled by a microhand. In addition, microassembly can be applied to building three-dimensional (3D) microsystems and devices [8]. However, the main difficulty of contact manipulation is releasing micro-objects adhering to the manipulator because of large adhesion forces. Thus, to release microobjects at the desired position, special releasing strategies are necessary [9–11]. For example, Kim et al. [9] utilized high speed motions of an end effector to release object on the desired position. Rong et al. and Takahashi et al. presented a vacuum tool and voltage control method for precise releasing [10, 11]. Moreover, it is difficult to deal

*Correspondence: kim@arai-lab.sys.es.osaka-u.ac.jp
†Eunhye Kim and Masaru Kojima contributed equally to this work
[1] Department of System Innovation, Osaka University, Osaka 560-8531, Japan
Full list of author information is available at the end of the article

with fragile objects, and contamination of the end effector is a weakness [12].

On the other hand, non-contact manipulation utilizes field forces without contact with the end effector, which makes the influence of adhesion forces negligible. For instance, Ding et al. and Guo et al. manipulated single particles and single cells by applying surface acoustic waves [13–15]. Grilli et al. [16] developed a dielectrophoretic method for trapping particles. Chung et al. [17] generated a stream by oscillating a bubble for 3D manipulation of microobjects. Nieuwstadt et al. [18] applied inertial lift force for sorting particles. The methods using field forces, including acoustic waves, the dielectrophoretic method, stream by bubble, and lift force, can manipulate multiple objects at the same time, but have difficulty in manipulating objects selectively. On the contrary, an optical tweezer can manipulate objects selectively, but cannot manipulate many objects simultaneously [19, 20]. However, non-contact manipulation cannot perform physical operation tasks, and complex systems are required for generating the aforementioned field forces.

Unlike the above-mentioned field forces, rotational stream can be generated by using only high-speed end effector motion. Our manipulator, actuated by three piezoelectric (PZT) actuators, is a suitable tool for generating swirl flow. In previous work, to manipulate objects using stream, many methods have been proposed. Tatsuno et al. [21] analyzed circulatory stream in two dimensions around an oscillating circular cylinder in one direction. Lee et al. manipulated multiple micro-objects using twin bubbles attached to a rod [22], and Chung et al. and Rogers et al. focused on manipulating a single object using acoustically oscillating bubbles [17, 23, 24]. They utilized the stream made by the oscillating bubbles, which can control the position of the objects. Hagiwara et al. generated a local streamline by high-frequency oscillation of a microtool in a microfluidic chip for cell manipulation . By tuning the oscillation parameter, they manipulated the cell in many different ways [25]. Hayakawa et al. extended this work to an open-chip environment by using micropillar patterns for cell transportation [26, 27]. However, these systems were analyzed only in a 2D plane. To manipulate microobjects in three dimensions, 3D rotational flow should be analyzed.

This paper presents a manipulator controlled by a parallel link. This mechanism can be applied to both contact and non-contact manipulation. We already manipulated microbeads and biological cells using a two-fingered microhand as a contact manipulation method in previous studies [2, 9]. In addition, we verified that this innovative manipulator generated local flow by using high speed motion of an end effector. We applied this local stream to release microobjects [28]. Our system generates rotational flow by circular motion using the parallel link; the method is applied to the non-contact manipulation of microbeads. In our previous work, Hattori et al. analyzed swirl flows by a glass needle vibration. They proposed a manipulator controlled by only one actuator for creating 2D circular vibration. They verified that the proposed manipulator can generate the rotational stream around the glass needle [29].

In this research, the main purpose is to find the relationship between the circular motion of an end effector and the velocity of the rotational flow. By changing the frequency (50, 77, 100 Hz) and the amplitude (12, 15, 21 μm) of the circular motion, the water flow is analyzed. From the experimental data using 9.6-μm microbeads and a theoretical model, we formulated two equations that can estimate the angular velocity of the rotational flow around the circular motion and the velocity toward the root of the end effector according to the frequency and the amplitude of the end effector. By using estimated velocities, we may control the velocity and position of a target object around the end effector precisely in 3D. For example, the speed of the target can be controlled by tuning the frequency and the amplitude of the end effector motion. In addition, the positioning of the target object can be managed by adjusting the performance time of the circular motion of the end effector. This proposed method has possibility to manipulate a lot of objects by generating of rotational flow and transporting the end effector together.

Methods

System setup for controllable motion

In this system, a manipulator composed of a parallel structure is utilized for generating 2D circular motion. The manipulator is controlled by two operating systems: a Windows PC and a Linux PC. The Windows PC provides visual feedback from a high-speed camera (Photron FASTCAM MC2). The Linux PC takes charge of the end effector's motion control by a parallel link actuated by three piezoelectric actuators (NEC TOKIN, AE0203D16). The end effector is composed of a glass needle. By heating and vertically pulling a glass rod (NARISHIGE G-1000) of a 90-mm in length and 1-mm in diameter, we made a sharpen glass needle which has about 23-mm in length, 1-mm in diameter, and less than 1-μm in diameter of tip of end effector.

For accurate positioning of microobjects using water flow, the precise high-speed motions of the end-effector is required. In this work, the target object is a 9.6 μm microbead around the end effector. To estimate the movement of the target, we can apply the rotational flow made by the circular motion. The rotational flow can be generated by the high speed motion (more than 50 Hz).

In addition, the flow velocity is changed by the frequency and the amplitude of the circular motion. Thus, the motion with high-accuracy (less than 1 μm) helps to formulate the velocity model clearly.

To generate high-speed motion with high-accuracy positioning, the parallel manipulator is a better solution than serial manipulator owing to its advantages such as high rigidity and positioning accuracy. Thus, we applied the parallel mechanism for this work. The parallel mechanism is a redesigned version of our previous structure [30]. The former version of the microhand was a 3-prismatic–revolute–spherical (PRS) parallel mechanism, while the current mechanism has a 3-prismatic–revolute–revolute (PRR) structure, which is smaller and more rigid. Details of this mechanism are described in [31]. Figure 1 shows the parallel link and the end effector's camera view. This mechanism is actuated by three piezoelectric actuators as prismatic joints to be extended up to 10.7 μm. The end-effector has three degrees of freedom: two rotational motions (X- and Z-movement) and one translational motion (Y-movement).

Figure 2 shows the control scheme of the parallel link for generating high-speed motion. The displacement of the three PZT actuators determines the 3D position of the end effector, which can be measured by the strain gauges attached to the actuators. The extensions of the PZT actuators are measured by the strain gauges fixed to each PZT actuator; the signals are transferred to the Linux PC through an amplifier (Kyowa MCD-16A) and an analog-to-digital board [Contec AD16-16(PCI)EV]. The 3D position of the end effector can be calculated using the obtained sensor data and compensated by a closed-loop PID controller. The desired voltage determined by computation of the sensor data is applied to each actuator through a digital-to-analog board [Contec DA16-16(LPCI)L] and an amplifier (MATSUSADA, HJPZ-0.15Px3). The desired end effector motion can be generated by using point-to-point movements of an end effector. This motion includes accelerating of the end effector to a necessary speed and decelerating to a stop. The sudden changes in acceleration or deceleration often create residual vibration. This residual vibration

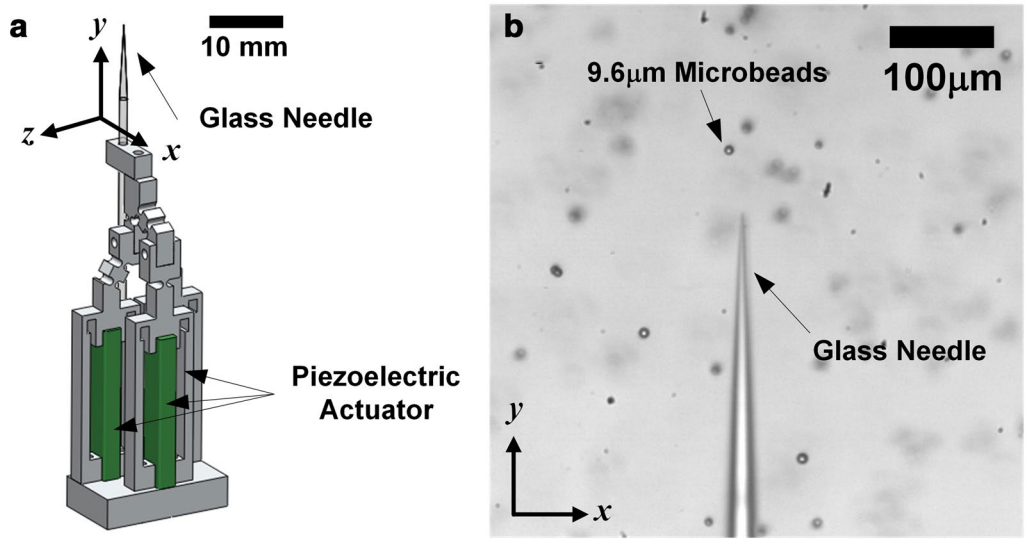

Fig. 1 **a** Cad model of a parallel link. **b** Camera view of an end-effector and microobjects

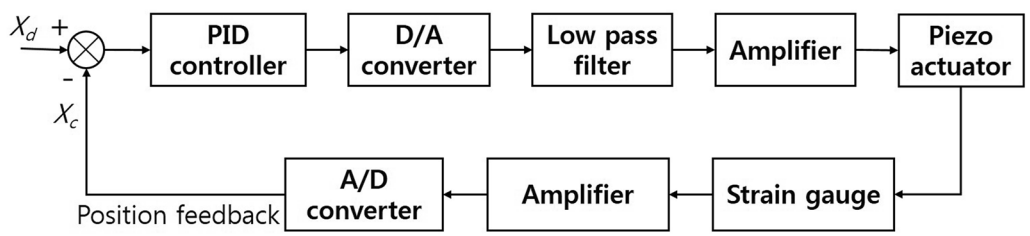

Fig. 2 Control scheme of the parallel link for manipulation

can be increased at the high speed motion because the high acceleration increases the abrupt changes of the end effector movement.

To generate the desired end effector motion precisely without the residual vibration, we fixed the length of the end effector at 16 mm and then carried out calibration by changing a calibration matrix. Generally, the longer the length of the end effector is, the more the vibration is. To suppress the vibration at high speed, it is better to select the length of end effector as short as possible. To generate a precise motion at high speed for formulating model clearly, we tried to suppress vibration less than 1 μm. We tested several lengths of end effector (14, 16, 18, 20, and 22 mm) and finally chose the length at 16 mm because the vibration is lower than 1 μm. As a result, we obtained an end-effector workspace of approximately 80 μm in X- and Z-directions and 10 μm in Y-direction. However, in high-speed motion (1 kHz), the vibration was still generated. To reduce the vibration of the end effector, a low-pass filter composed of an RC circuit was applied. Thus, the vibration at the high frequency of 1 kHz was remarkably reduced from over 5 μm to less than 0.5 μm. In this system, the maximum amplitude is approximately 24 μm in the X- and Z-directions at the maximum frequency (1 kHz).

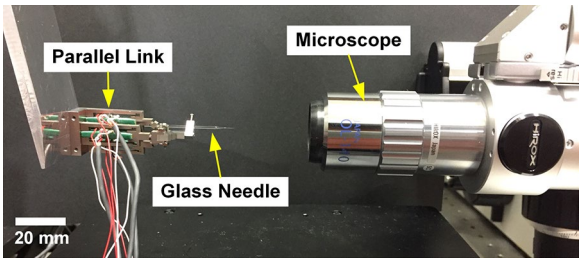

Fig. 3 Experimental setup for observing the motion of the end effector

Circular motion of the end effector

To analyze the rotational flow in 3D space, generation of circular motion is mandatory. Using the parallel link, circular motions with different amplitudes and frequencies can be created. The circular motion is designed by the combination of a sine function in the X-direction and a cosine function in the Z-direction. The motion consists of ten steps to make this motion as close as possible to a circular shape. The maximum frequency of the circular motion is 100 Hz because the number of steps is ten and the maximum frequency of the end effector during a step is 1 kHz. After generating 2D circular motion, we observed the end-effector's motion in the XZ plane through a microscope (Hirox, CX-10C) with a objective lens (OL-140). The experimental setup for observing the circular motion in the XZ plane is shown in Fig. 3.

The motions of the end effector with different parameters were observed. To compare the swirl flow according to amplitude of the end effector, we applied several amplitudes (12, 15, and 21 μm) by holding the frequency constant. We also changed the frequencies from 100 Hz (maximum frequency) to 10 Hz. Figure 4 shows the high-speed motions of the end effector (100 Hz) in different amplitudes captured by a high-speed camera. From these figures, we can see the circular shape with different diameters. From the observed images, we can verify that the concise parallel link is a suitable tool for creating 2D circular motion.

The motions of the end effector with different parameters were observed. To compare the rotational flow according to amplitude of the end effector, we applied several amplitudes (12, 15, and 21 μm) by holding the frequency constant. We also changed the frequencies from 100 Hz (maximum frequency) to 10 Hz. Figure 4 shows the high-speed motions of the end effector (100 Hz) in different amplitudes captured by a high-speed camera. From these figures, we can see the circular shape with different diameters. From the observed

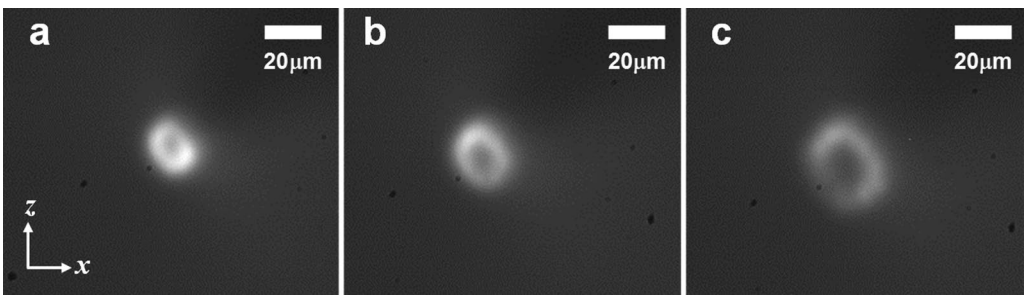

Fig. 4 High-speed circular motion of the end effector for different amplitudes. The frequency is 100 Hz and the amplitude is **a** 12 μm, **b** 15 μm, **c** 21 μm

images, we can verify that the concise parallel link is a suitable tool for creating 2D circular motion.

Experimental setup for analyzing rotational flow

In this section, the experimental setup for analyzing the rotational flow is described. To verify that the circular motion can generate rotational flow around the end effector, the experiment was conducted using 9.6-μm microbeads in water. By using 9.6-μm microbeads, we can extend this research to the cell manipulation in the future. The experimental setup is shown in Fig. 5. The water stream was observed by a microscope (IX71) with a 10× objective lens that provided a visual space of 512 μm × 512 μm. A high-speed camera that can capture images at 2000 frames per second was applied for tracking the microbeads at high speed. The density and dynamic viscosity of water are 998.2 kg/m^3 and 1.003 × 10^{-3} kg/m s, respectively, at 20 °C [32]. The experiments were executed 250 μm above the substrate.

First, we applied several frequencies (100, 77, 50, 40, 33, and 10 Hz) at a fixed amplitude (21 μm) in order to determine the range of frequencies that can generate a rotational stream. At frequencies lower than 50 Hz, the rotational flow was not observed. On the other hand, when the frequency of the circular motion was 50 Hz or more, the rotational flow was detected despite the same amplitude of the circular motion. The water flow when the end-effector was rotating in a circle at a frequency of 100 Hz is shown in Fig. 6. The images were captured every 0.028 s. A microbead is tracked and the path of the object is shown. As shown in Fig. 6, the microbead is rotating around the end-effector as well as moving toward the root of the end-effector. From the experimental result, we found that the circular motion of the glass needle generates the rotational stream in three dimensions and the low frequency (less than 50 Hz) of the circular motion cannot create the rotational flow. Thus, we utilized three frequencies (50, 77, and 100 Hz) for the experiments. Supplementary video (Additional file 1) shows the rotational flow by the circular motion with three frequencies and amplitudes. From this movie, we can verify that the circular motion of the end effector makes the rotational flow that can control microobjects.

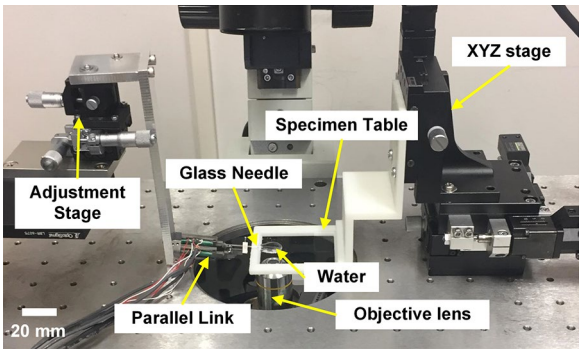

Fig. 5 Experimental setup

Rotational flow by circular motion

In the previous section, we observed the rotational stream by the circular motion when the frequency was 50 Hz or higher. In addition, the microbeads rotated by the circular motion were not only rotated around the end effector but also moved to the root of the end effector. As a result, the rotational flow can be analyzed by two relationships: the relationship between the angular velocity and the distance from the center of the end effector's motion, and the relationship between the velocity toward the root of the end effector and the distance from the center of the end effector's motion.

Figure 7a shows the measurement method of the rotational stream in 3D space. In Fig. 7b, the blue circle indicates the initial position of the microbead and the red circle shows the position of the microbead after one turn (after 0.16 s). Positions in the X-direction of the two circles are almost on the same axis, and the Y-direction is changed. In addition, the distances from the center of the circular motion (r_1 and r_2) are the same. From this trajectory of the microbead, we can verify the relationship between the flow velocity in three dimensions and the radius of the flow (Fig. 7a). The angular velocities and the velocities toward the root of the end effector can be calculated by the movements of the 9.6-μm microbeads and the time it takes for the object to traverse half a revolution. To be specific, we computed the radius of rotation described in Fig. 7 (r_1 and r_2) using the movement of the object in the X-direction after a half-turn. The angular velocity and the velocity toward the root of the end effector were calculated by the time it takes for the microbead to make a half-turn and the moving distance in the Y-direction, respectively. Experiments were conducted by changing the frequency and the amplitude of the end effector. In this experiment, we utilized a cone shape of a glass needle. Generally, the thicker the end effector is, the faster the velocity is [26]. Thus, to minimize this influence, we selected a specific region having similar diameter from 8 to 12 μm. The trapped region in Fig. 7b shows the selected region. It is approximately from 80 to 250 μm from needle tip.

Angular velocity of rotational flow

Vortex theory

To analyze a simple model for a vortex, Rankine's combined vortex was utilized. A vortex is classified as either a forced vortex or a free vortex. The angular velocity of a forced vortex is constant regardless of the radius of

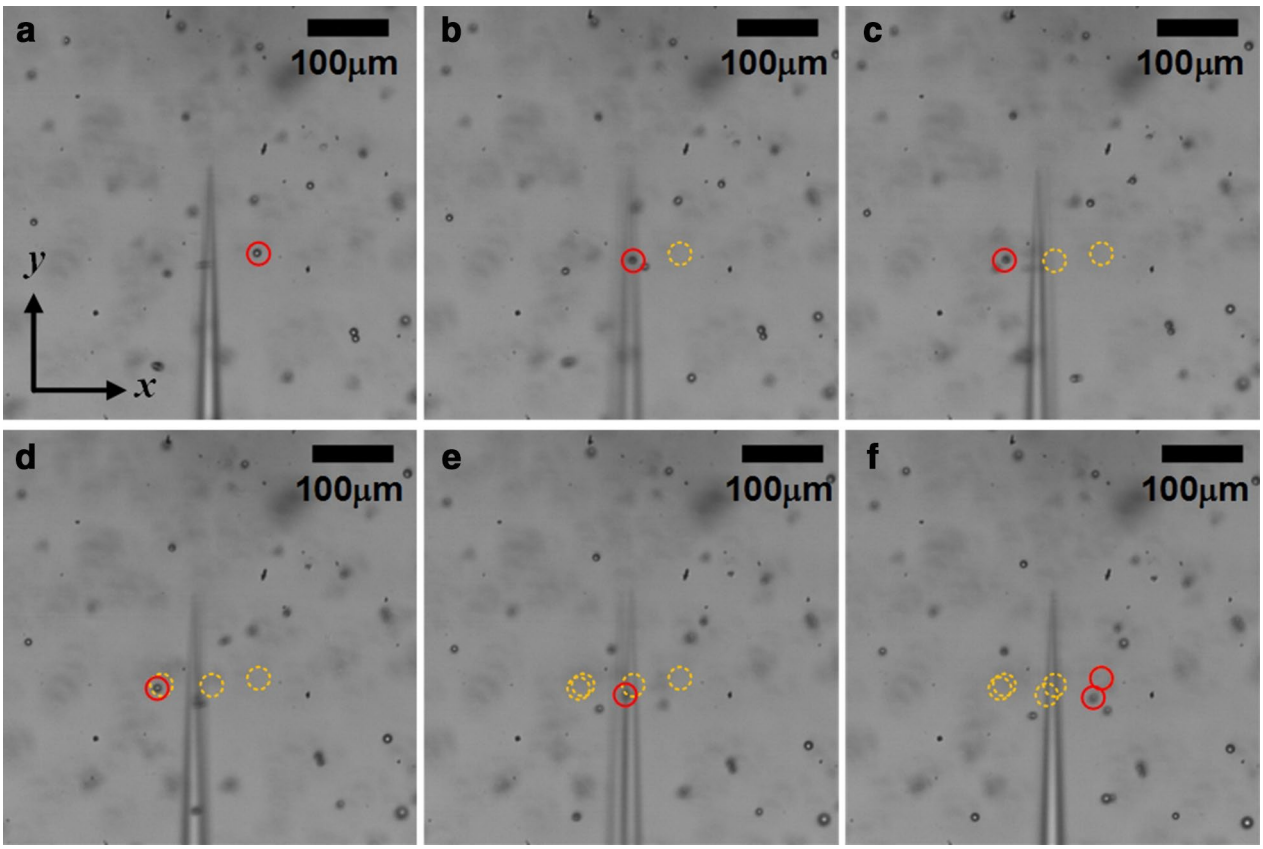

Fig. 6 Rotational flow by the circular motion at 100 Hz. The microbead is tracked when the end-effector is rotating in 100 Hz. **a** Initial position, **b** 0.028 s, **c** 0.056 s, **d** 0.084 s, **e** 0.112 s, **f** 0.14 s

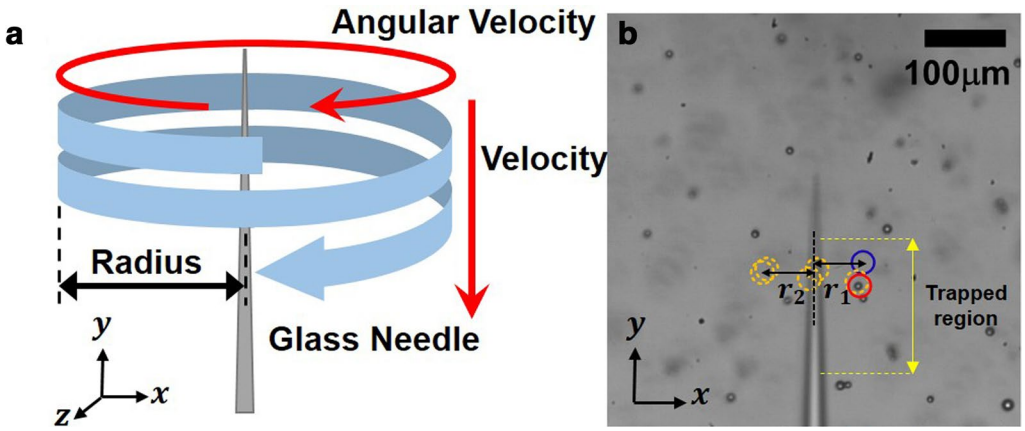

Fig. 7 Measurement method of rotational stream in 3D space. **a** Measurement method of flow velocities. **b** Trajectory of a microbead by the rotational stream

the flow, whereas the angular velocity of a free vortex is inversely proportional to the square of the radius of the vortex. In our system, we generated the vortex by the circular motion of an end effector. The result is a forced vortex in the center surrounded by a free vortex. Because our purpose is to measure the angular velocity around the circular motion, Rankine's combined model for the free vortex can be applied to our system.

Experimental results

Figure 8 shows the relationship between the angular velocity of the rotational flow and the distance from the center of the end-effector's motion (radius). Three frequencies (50, 77, and 100 Hz) and amplitudes (12, 15, and 21 μm) were utilized. To find a relationship between the angular velocity and the radius, the frequency and the amplitude of the end effector were changed. From the experimental results, we found several things. The larger the radius of rotation, the slower the angular velocity in every case. In addition, the larger the amplitude and frequency of the end effector, the faster the angular velocity. From the experimental result, we can conclude that the angular velocity can be controlled by changing the amplitude and the frequency of the end effector. However, with only the plotted experimental data, it is difficult to estimate the angular velocity according to the three parameters of amplitude, frequency, and radius in detail.

A model to formulate the experimental results

In this section, a simple model that can easily and quickly calculate the angular velocity despite the several variables is proposed. To formulate an equation, first, Rankine's combined model was applied. From this model, a simple equation can be established as (1) because the angular velocity of the free vortex in this model is inversely proportional to the square of the radius of the vortex. The constant (C) is a temporary value and r is a radius of the rotational flow.

$$\omega = \frac{C}{r^2} \tag{1}$$

To fix the temporary value (C), we applied the nonlinear regression model to the experimental data [33]. To derive the equation, we defined the dependent and independent variables, as well as parameters that help to define the properties of the model. In this

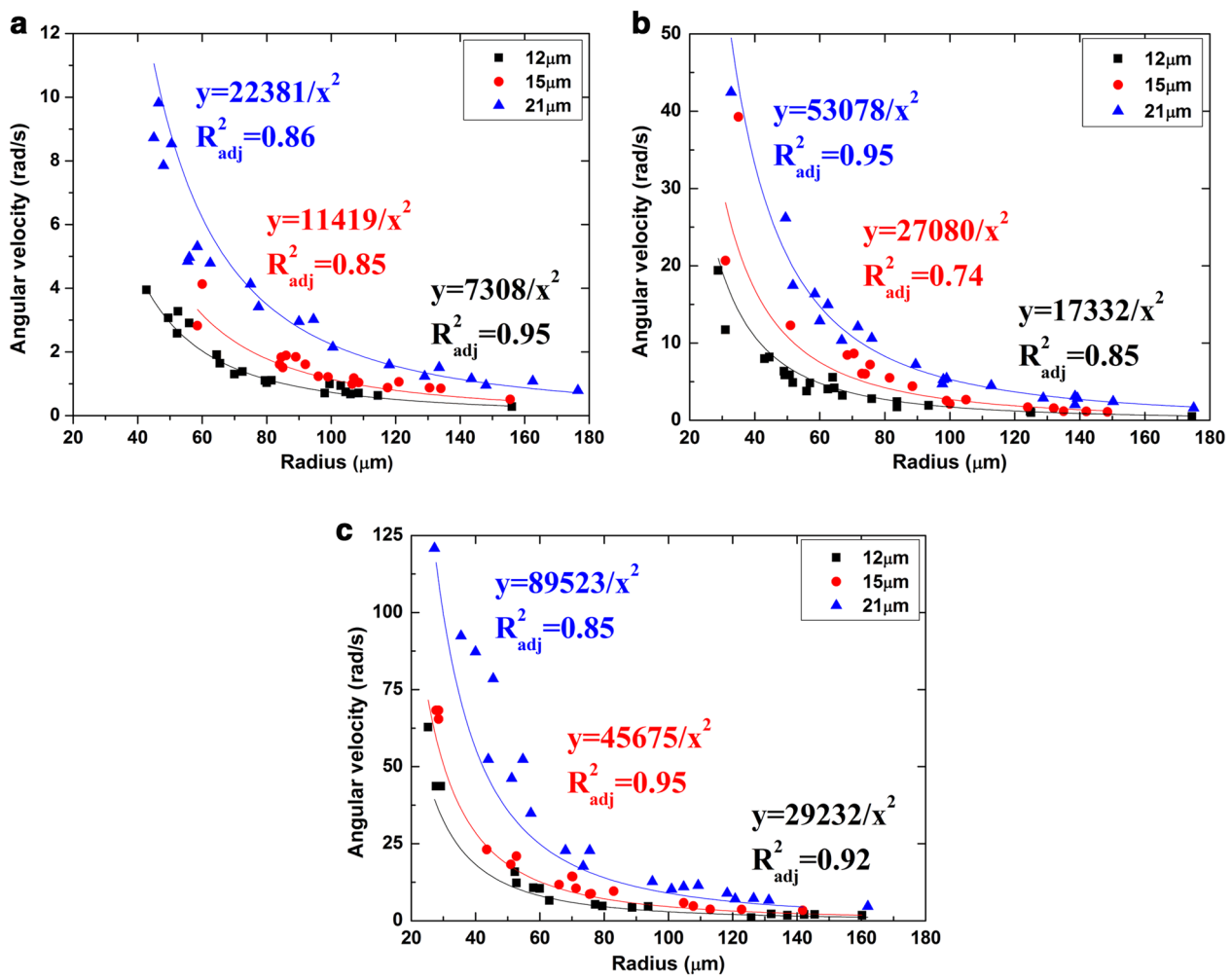

Fig. 8 Relationship between the radius and angular velocity of the rotational flow with a fitting curve. The frequency is **a** 50 Hz, **b** 77 Hz, and **c** 100 Hz

experiment, the dependent variable is the angular velocity, and the independent variables are the radius of the flow, the end-effector frequency, and the end-effector amplitude. To find the relationship between the temporary constant and the independent variables (amplitude and frequency), the experimental result was empirically fitted. Therefore, Eq. (2) can be established:

$$\omega = C_1 \frac{f^2 A^2}{r^2} \tag{2}$$

f and A indicate the end-effector frequency and the amplitude, respectively. r is the radius of the stream and C_1 is the rate constant. It is difficult to determine the rate constant (C_1) because the constant should be applicable to all of the experimental data having different variables. To search for a suitable constant (C_1), we computed the correlation between the observed values from the experiments and the predicted values from the computation of the equation. We drew fitting curves by substituting an arbitrary constant for every case, and compared the curve with actual plotted data. To analyze the goodness-of-fit of the curve, the correlation was computed by comparing an adjusted R-squared ($\bar{R}^2$). If the adjusted R-squared is close to 1.0, a linear relationship is reasonable and the fitting equation would be in accordance with the data. In addition, if the value ($\bar{R}^2$) is more than 0.7, the proposed model can be applied to estimate the values. The adjusted R-squared is largest (0.88) when the constant (C_1) is 0.0203. Thus, 0.0203 was selected as the rate constant. In Fig. 8, the values of adjusted R-squared are shown for different amplitudes and frequencies when the constant is 0.0203. The average of the values is approximately 0.88 and every value is larger than 0.74, which means that the data is well fitted by Eq. (2). Figure 8 shows the experimental data and the fitting curves calculated by the equation.

From the proposed model, we found several things. First, the angular velocity is inversely proportional to the square of the radius of the stream. This result shows that our experimental data follows Rankine's combined vortex model. Second, the angular velocity is proportional to the square of the end-effector amplitude. Third, the angular velocity is also proportional to the square of the end-effector frequency. These analyses mean that we can precisely control the velocity of the stream around the end effector by tuning the frequency and the amplitude of the end effector's motion. Furthermore, we can predict the angular velocity at a different frequency or amplitude using only the simple model we propose.

Flow velocity toward the root of the end effector

Experimental results

Figure 9 shows the relationship between the radius of the rotational flow and the velocity in the Y-direction by changing the end-effector frequency and amplitude. Three frequencies (50, 77, and 100 Hz) and three amplitudes (12, 15, and 21 μm) were applied to analyze the relationship in detail. From these experiments, we obtained several results. First, the larger the radius of rotational flow, the lower the velocity in the Y-direction. Second, the larger the amplitude of the end effector, the faster the velocity in the Y-direction. Finally, the higher the frequency of the end effector, the faster the velocity in the Y-direction. However, as discussed in the previous section regarding the angular velocity, with only the plotted velocity data, it is too difficult to analyze the relationship between the velocity in the Y-direction and the radius of the rotation depending on the end-effector frequency and amplitude. Thus, we propose a model that can show the relationship clearly.

Analysis of experimental results

To find a simple model to describe the experimental results, we applied the nonlinear regression model by fitting the data set and then evaluated the fitted curve by calculating the correlation coefficient between the original data and the fitting curve. The experimental result was empirically fitted to estimate the velocity toward the root of the end effector. To estimate the velocity according to the end-effector frequency and amplitude in detail, several variables were utilized. The frequency, amplitude, and radius were used as independent variables to find the equation of velocity in the Y-direction. As a result, Eq. (3) and the fitting curves in Fig. 9 were obtained.

$$v_y = \frac{C_2 f^{2.2} A + C_3 f^{2.7}}{r} \tag{3}$$

C_2 and C_3 indicate the rate constant, and r is the radius of the rotational stream. f and A represent the end-effector frequency and amplitude, respectively. From the equation determined by the fitted curves, the result that the velocity is inversely proportional to the radius of the flow is readily shown and we can estimate the velocity at different frequencies and amplitudes. To verify the model, we calculated the correlation between the observed values from the experiments and the predicted values by the model using the adjusted R-squared ($\bar{R}^2$). We adjusted the rate constants (C_2 and C_3) to find the best-fitting curve for this model. When C_2 and C_3 are 0.0355 and −0.034, respectively, the adjusted R-squared is largest, so we selected these values as the rate constant. Figure 9 shows the values of adjusted R-squared according

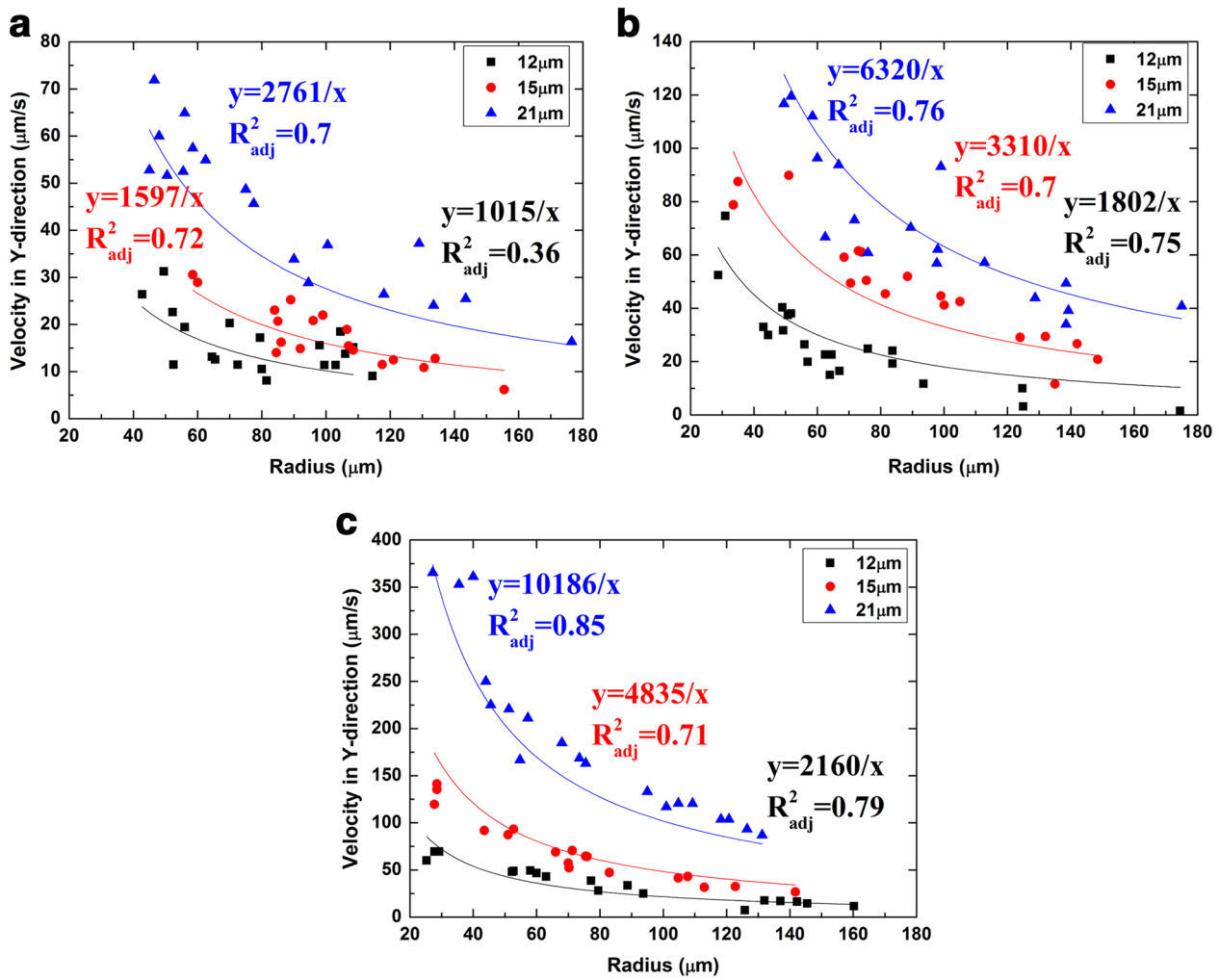

Fig. 9 Relationship between the radius and the velocity toward the root of the end-effector with fitting curve. The frequency is **a** 50 Hz, **b** 77 Hz, and **c** 100 Hz

to the end-effector frequency and amplitude. The average of the values is approximately 0.704, which means the fitted curves and proposed model are applicable for estimating the velocity in the Y-direction. However, at the frequency of 50 Hz and amplitude of 12 μm, the correlation is lower than in other cases. In this case, it is difficult to measure the exact distance because the moving distance of the microbead in the Y-direction is small when the object traverse half a turn. From these fitting models, we conclude that the velocity toward the root of the end effector is inversely proportional to the distance from the center of the end effector's circular motion, in addition, we can calculate and predict the velocity in the Y-direction if the end-effector frequency and amplitude are known.

Discussion

Analysis of rotational flow is a vital step for 3D micromanipulation. The final goal of the research is 3D manipulation of multiple objects. The first step is to control the position and speed of a single object precisely using the rotational flow by only one end effector. The next step is 3D manipulation of multiple objects simultaneously as a group by transporting the end effector. To manipulate multiple objects together, we focused on rotational flow that can trap and transport many objects at the same time.

To generate the stream precisely, we analyzed the rotational flow in detail by changing the frequency and the amplitude. To analyze the flow, the first step is generation of precise end-effector motion. To generate accurate

motion, we used a compact parallel link and succeeded in creating circular motion with different amplitudes and frequencies. As the next step, we formulated two equations by the angular velocity in the XZ-plane and the velocity in the Y-direction. Using these models, we can control the velocity of the rotational flow precisely by tuning the end effector's motion.

Using proposed equations, we could control the speed and position of a target object precisely by controlling an end effector motion. The rotational flow could control the speed of an object around the end effector by changing the frequency and the amplitude of the circular motion and then determine the final position by managing the performance time of the motion. In addition, we will extend flow control to the manipulation of multiple objects. The manipulation procedure is descried in Fig. 10. In order to trap and transport multiple objects at the same time, first, an end-effector generates a rotational flow around the target objects (Fig. 10b) and subsequently the end effector is transported to the desired location by the stage while maintaining the circular motion (Fig. 10c). Finally, the end effector stops the circular motion when the targets reach the desired position (Fig. 10d).

However, it is difficult to control two flow in the XZ-plane and in the Y-direction simultaneously. It has a possible method. We might keep the position in the Y-direction by transporting the end effector in the opposite direction. The transportation of the end effector in the Y-direction might be offset the flow movement in the Y-direction.

For generating rotational flow, we tested several frequencies. As the result, we concluded that the frequencies more than 50 Hz can generate the rotational flow and control the microbeads. Insufficient force could be a possible reason. The end effector motion generates the drag force that can manipulate the objects. This drag force cause the object to move along with the flow. If the enough drag force is not generated by the end effector motion, the object will not move with the flow. Based on the Stoke's drag assumption [32], we can estimate the force. η, R, and V are the dynamic viscosity of water, radius of object, and fluid velocity, respectively.

$$F_d = 6\pi\eta RV \tag{4}$$

To compare the force at the different frequency, we set the same amplitude of 21 μm and the same distance of 50 μm. The forces are 0.0425 nN at the frequency of 50 Hz and 0.0272 nN at the frequency of 40 Hz. From this result, we could predict that the force at the frequency of 40 Hz is not enough to manipulate the 9.6 μm microbeads.

This drag force also applied to estimate the size effect of object. By calculating the drag force using (4) and buoyant force ($F_b = \rho V_f g$, where ρ is the density of the water, V_f is the volume of the object, and g is the acceleration due to gravity), we could predict the movement of the different size of objects. Generally, the larger the diameter of the object is, the more the buoyant force and drag force is. However, the rate of increase is different. To compare the different size of objects, we use the same parameters, such as frequency (50 Hz), amplitude (21 μm) and distance from end effector (50 μm). As a result, at the diameter of the 10 μm, the drag force is 0.043 nN and buoyant force is 5.12×10^{-3} nN. At the diameter of the 25 μm, the drag and buoyant force are 0.106 and 0.08 nN, respectively. At these two cases, the drag force is larger the buoyant force and then the objects could be moved along with the flow. Our target object, NIH3T3 cell (18 μm in diameter [34]), could be moved with the flow. However, when the diameter is 30 μm, the buoyant force (0.138 nN) is larger than the drag force (0.128 nN). The difference between two forces is gradually increased as the diameter is increased. In this case, it is highly possible that the end effector could not manipulate the object.

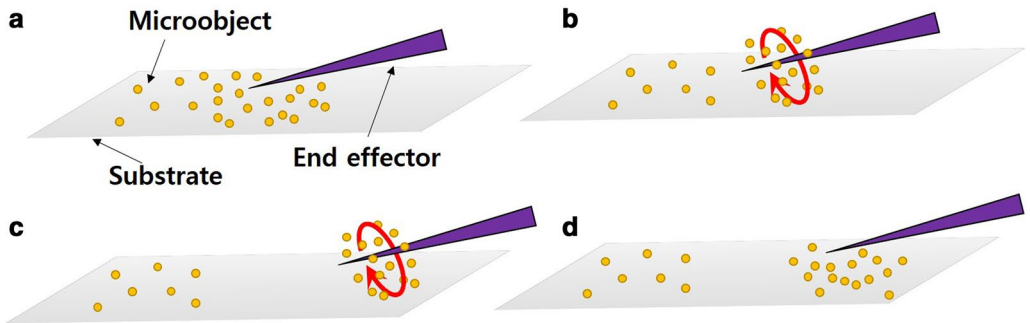

Fig. 10 Manipulation procedure of multiple objects. **a** Approach to target objects. **b** Trap target objects by generating rotational flow. **c** Transport targets by moving stage. **d** Place targets to the desired position by stopping the end effector's motion

In the future, we will manipulate various sizes of objects including NIH3T3 cells by adding the detail force model to our method. In a water environment, the forces such as drag, buoyancy, and gravity are critical factors for precise manipulation. Small objects and large objects have different physical characteristics, such as mass and size, and therefore the force model should be calculated depending on the physical properties.

Conclusions

We have analyzed the rotational flow generated by the circular motion of an end effector in water. Generation of swirl flow was attained by a compact parallel link actuated by three piezoelectric actuators. Using the parallel link, we succeeded in generating circular motion with different amplitudes and frequencies. From the rotational flow by the circular end-effector motion, we found the range of frequencies that can generate swirl flow and then selected several frequencies (50, 77, and 100 Hz) and amplitudes (12, 15, and 21 μm) to analyze the flow velocity. The flow velocity was analyzed in 3D space by changing the amplitude and the frequency. The flow was analyzed in two directions: velocity in the Y-direction and the angular velocity in the XZ-plane around the end effector. From the experimental results and vortex theory, we formulated simple equations to analyze the flow velocity precisely and easily. To verify the models, we computed the correlation between the observed data from the experiments and the predicted data from the equations using the adjusted R-squared. As a result, we can precisely control the rotational flow by tuning the frequency and the amplitude of the end effector. In the future, we will apply the analysis to 3D manipulation of many objects simultaneously.

Additional file

Additional file 1. Rotational flow by circular motion with differentfrequencies and amplitudes. The movie shows the movement of microbeads along with rotational flowby circular motion with different frequencies and amplitudes.

Authors' contributions

EK initiated the conceptual idea, implemented, conducted the experiments, gathered and analyzed data, and drafted the manuscript. MK helped to initiate the concept, provided facility and technical support, and helped to revise the manuscript. LX and TH helped to conduct the experiments and analyze data. KK and YM provided technical advises, and helped to revise the manuscript. AT revised the concept, provided all support and advises, and helped to revise the manuscript. All authors read and approved the final manuscript.

Author details

[1] Department of System Innovation, Osaka University, Osaka 560-8531, Japan. [2] School of Mechatronical Engineering, Beijing Institute of Technology, Beijing 100081, China.

Acknowledgements

This work was supported by Grant-in-Aid for Scientific Research on Innovative Areas "Bio Assembler" (JP23106005) and Grant-in-Aid Scientific Research (A) (JP16H02321) from the Ministry of Education, Culture, Sports, Science and Technology of Japan.

Competing interests

The authors declare that they have no competing interests.

Received: 7 December 2016 Accepted: 1 February 2017
Published online: 14 February 2017

References

1. Savia M, Koivo HN (2009) Contact micromanipulation—survey of strategies. IEEE/ASME Trans Mechatron 14(4):504–514
2. Avci E, Ohara K, Nguyen CN, Theeravithayangkura C, Kojima M, Tanikawa T, Mae Y, Arai T (2015) High-speed automated manipulation of microobjects using a two-fingered microhand. IEEE Trans Ind Electron 62(2):1070–1079
3. Zhang Y, Chen BK, Liu XY, Sun Y (2010) Autonomous robotic pick-and-place of microobjects. IEEE Trans Robot 26(1):200–207
4. Chen BK, Zhang Y, Sun Y (2009) Active release of microobjects using a MEMS microgripper to overcome adhesion forces. J Microelectromechanical Syst 18(3):652–659
5. Yamanishi Y, Kuriki H, Sakuma S, Onda K, Arai F (2012) Local ablation by micro-electric knife. In: 7th IEEE international conference on nano/micro engineered and molecular systems (NEMS), 2012, IEEE, New York, pp 129–132
6. Huang HB, Sun D, Mills JK, Cheng SH (2009) Robotic cell injection system with position and force control: toward automatic batch biomanipulation. IEEE Trans Robot 25(3):727–737
7. Motoyoshi T, Kojima M, Ohara K, Horade M, Kamiyama K, Mae Y, Arai T (2015) Development of a real-time local environment stimulation system with visual feedback control. In: 2015 IEEE international conference on robotics and automation (ICRA), IEEE, New York, pp 4036–4041
8. Tamadazte B, Piat NLF, Dembélé S (2011) Robotic micromanipulation and microassembly using monoview and multiscale visual servoing. IEEE/ASME Trans Mechatron 16(2):277–287
9. Kim E, Kojima M, Kamiyama K, Horade M, Mae Y, Arai T (2015) Releasing and accurate placing of adhered micro-objects using high speed motion of end effector. In: 2015 IEEE/RSJ international conference on intelligent robots and systems (IROS), IEEE, New York, pp 2006–2011
10. Rong W, Fan Z, Wang L, Xie H, Sun L (2014) A vacuum micrograpping tool with integrated vibration releasing capability. Rev Sci Instrum 85(8):085002
11. Takahashi K, Kajihara H, Urago M, Saito S, Mochimaru Y, Onzawa T (2001) Voltage required to detach an adhered particle by coulomb interaction for micromanipulation. J Appl Phys 90(1):432
12. Vandaele V, Lambert P, Delchambre A (2005) Non-contact handling in microassembly: acoustical levitation. Precis Eng 29(4):491–505
13. Shi J, Ahmed D, Mao X, Lin SCS, Lawit A, Huang TJ (2009) Acoustic tweezers: patterning cells and microparticles using standing surface acoustic waves (ssaw). Lab Chip 9(20):2890–2895
14. Ding X, Lin SCS, Kiraly B, Yue H, Li S, Chiang IK, Shi J, Benkovic SJ, Huang TJ (2012) On-chip manipulation of single microparticles, cells, and organisms using surface acoustic waves. Proc Natl Acad Sci 109(28):11105–11109
15. Guo F, Mao Z, Chen Y, Xie Z, Lata JP, Li P, Ren L, Liu J, Yang J, Dao M (2016) Three-dimensional manipulation of single cells using surface acoustic waves. Proc Natl Acad Sci 113(6):1522–1527
16. Grilli S, Ferraro P (2008) Dielectrophoretic trapping of suspended particles by selective pyroelectric effect in lithium niobate crystals. Appl Phys Lett 92(23):232902
17. Chung SK, Cho SK (2009) 3-d manipulation of millimeter-and micro-sized objects using an acoustically excited oscillating bubble. Microfluid Nanofluidics 6(2):261–265

18. Nieuwstadt HA, Seda R, Li DS, Fowlkes JB, Bull JL (2011) Microfluidic particle sorting utilizing inertial lift force. Biomed Microdevices 13(1):97–105
19. Grier DG (2003) A revolution in optical manipulation. Nature 424(6950):810–816
20. Hu S, Sun D (2011) Automated transportation of single cells using robot-tweezer manipulation system. J Assoc Lab Autom 16(4):263–270
21. Tatsuno M (1973) Circulatory streaming around an oscillating circular cylinder at low reynolds numbers. J Phys Soc Jpn 35(3):915–920
22. Lee JH, Lee KH, Chae JB, Rhee K, Chung SK (2013) On-chip micromanipulation by AC-EWOD driven twin bubbles. Sens Actuators A Phys 195:167–174
23. Rogers P, Neild A (2011) Selective particle trapping using an oscillating microbubble. Lab Chip 11(21):3710–3715
24. Park IS, Shin JH, Lee YR, Chung SK (2016) On-chip micromanipulation using a magnetically driven micromanipulator with an acoustically oscillating bubble. Sens Actuators A Phys 248:214–222
25. Hagiwara M, Kawahara T, Arai F (2012) Local streamline generation by mechanical oscillation in a microfluidic chip for noncontact cell manipulations. Appl Phys Lett 101(7):074102
26. Hayakawa T, Sakuma S, Fukuhara T, Yokoyama Y, Arai F (2014) A single cell extraction chip using vibration-induced whirling flow and a thermo-responsive gel pattern. Micromachines 5(3):681–696
27. Hayakawa T, Sakuma S, Arai F (2015) On-chip 3d rotation of oocyte based on a vibration-induced local whirling flow. Microsyst Nanoeng 1:1–9
28. Kim E, Kojima M, Kamiyama K, Horade M, Mae Y, Arai T (2015) Releasing of adhered micro-objects using local stream generated by high speed motion of end effector. In: 2015 IEEE international conference on mechatronics and automation (ICMA), IEEE, New York, pp 1036–1041
29. Hattori T, Kamiyama K, Kojima M, Horade M, Mae Y, Arai T (2015) Generation of swirl flow by needle vibration for micro manipulation. In: 2015 IEEE/RSJ international conference on intelligent robots and systems (IROS), IEEE, New York, pp 772–777
30. Ramadan AA, Takubo T, Mae Y, Oohara K, Arai T (2009) Developmental process of a chopstick-like hybrid-structure two-fingered micromanipulator hand for 3-d manipulation of microscopic objects. IEEE Trans Ind Electron 56(4):1121–1135
31. Kurata T, Avci E, Kamiyama K, kojima M, Ohara K, Horade M, Ejima T, Tanikawa T, Mae Y, Arai T (2014) Vibration reduction of microhand used in transporting operations. In: 2014 international symposium on flexible automation, pp 1–6
32. Gauthier M, Régnier S, Rougeot P, Chaillet N (2006) Analysis of forces for micromanipulations in dry and liquid media. J Micromechatron 3(3):389–413
33. Motulsky H, Christopoulos A (2004) Fitting models to biological data using linear and nonlinear regression: a practical guide to curve fitting. OUP, Oxford
34. B10NUMB3R5: the database of useful biological numbers. http://www.bionumbers.hms.harvard.edu. Accessed 16 Jan 2017